AIChE WILEY InterScience DISCOVER SOMETHING GREAT

Simulation of Mixing Dynamics in Agitated Pulp Stock Chests using CFD

C. Ford, F. Ein-Mozaffari, C. P. J. Bennington, and F. Taghipour
Dept. of Chemical and Biological Engineering, Pulp and Paper Centre, University of British Columbia, 2385 East Mall, Vancouver, BC V6T 1Z4 Canada

DOI 10.1002/aic.10958
Published online September 5, 2006 in Wiley InterScience (www.interscience.wiley.com).

Agitated-pulp chests function as low-pass filters to reduce high-frequency variability in pulp properties (mass concentration, freeness, and so on) ahead of many pulping and papermaking operations. Tests on both industrial and scale-model chests have shown that their dynamic performance is far from ideal, with a significant extent of nonideal flow (short circuiting, recirculation and stagnation) possible. The flow field of a 1:11 scale-model pulp chest was modeled using a commercial computational fluid dynamics (CFD) software package (Fluent) with the pulp suspension treated as a modified Bingham plastic. A multiple reference frame approach was used with coupling between reference frames made using a velocity transformation. The flow profiles predicted by the simulation agreed qualitatively with those observed in the experiments. The power input predicted by the simulations was slightly higher (about 12%) than that measured. The velocity field obtained from the CFD model was used to obtain the system's dynamic response to a frequency-modulated random binary input signal. These data were then used as input to a dynamic model that treated flow within the chest as following two streams: one bypassing the mixing zone and one entering it. For both streams, the fraction of suspension passing through each zone was determined and a time constant and delay time computed. These parameters were then compared to those measured experimentally under identical operating conditions. The CFD simulation provides detailed information on the velocity profile within the chest and allows the location(s) of poor mixing regions to be identified. © 2006 American Institute of Chemical Engineers *AIChE J,* 52: 3562–3569, 2006
Keywords: pulp suspensions, mixing, suspensions, computational fluid dynamics (CFD)

Introduction

Mixing is a key unit operation in many chemical processes. In the pulp and paper industry, effective mixing is critical for the success of several operations including the blending of different pulp stocks in papermaking, consistency control ahead of paper machines, and steam addition and chemical contacting with pulp in bleaching stages.

Agitated pulp stock chests function as low-pass filters to reduce high-frequency variability in pulp properties, such as the mass concentration and freeness ahead of many pulping and papermaking operations. This complements the action of control loops which can only control low-frequency variability below the control loop cut-off frequency.[1] In spite of the importance of these applications, the problem of designing and scaling-up agitated stock chests has been tackled mainly by means of semiempirical methods. One common design method has been summarized by Yackel[2], and is based on matching the momentum flux generated by an impeller with that needed to provide complete motion in the chest. Using Yackel's definition, "complete motion" occurred when the suspension was in motion over the entire top surface of the mixing vessel. This definition agreed with that used in previous work on the design of paper stock mixers.[3]

Ein-Mozaffari et al.[4] studied the dynamics of pulp agitation using a 1:11 scale-model Plexiglas chest equipped with a side

Correspondence concerning this article should be addressed to C. P. J. Bennington at cpjb@chml.ubc.ca.

© 2006 American Institute of Chemical Engineers

entering impeller. They found that even when complete surface motion was attained, considerable channeling, recirculation and stagnation existed below the suspension surface. Dynamic studies made in industrial chests confirmed these findings.[5] In a number of cases, the suspension volume involved in active mixing was only 20 to 40% of that in the chest. Consequently, the degree of variability reduction was considerably poorer than that of a perfectly mixed chest and was attributed to the stagnant and poor mixing zones. The undesirable flows responsible for this occur because of the complex rheology of the pulp suspensions.

Pulp suspensions are non-Newtonian fluids. They are continuous fiber networks that possess structure and strength resulting from interaction between neighboring fibers. To create motion throughout the suspension, the shear stresses imposed on the suspension must be greater than the network strength which is measured as the suspension yield stress. Pulp suspensions are often treated as plastic materials; they show little deformation up to the yield stress and only flow once the yield stress is exceeded. Fiber suspensions also exhibit nonlinear viscoplastic properties, such as shear thinning,[6] although, after yield-point, pulp suspensions display unique rheology that is not well characterized.[7]

A significant improvement in the design of agitated stock chests could be obtained by developing robust models that consider the actual flow field inside the vessel. Computational fluid dynamics (CFD) makes the development of these models possible by solving the momentum and mass conservation equations that govern the flow in the agitated chest. Significant effort has been made over the past decade toward the development of reliable CFD models for mixing, including development of sophisticated turbulence models, and new methods to accurately model rotating flows. In particular, the development of the sliding mesh, multiple reference frame, and mixing plane methods make it possible to perform numerical simulations that include the impeller region in the computational domain instead of imposing boundary conditions at the impeller location. In the latter case the model can only be extended to geometries close to that for which the experimental data were obtained.[8]

Bakker and Fasano[9] were the first to model the pulp flow in a stock chest with a side entering impeller using CFD. The impeller was simulated by defining a flat velocity profile at the impeller location, and a combination of turbulent and laminar-flow regimes were used in the tank. The rheological model used for the pulp suspension was not specified in detail and the simulation results were only compared to visual observations of the flow field, with which the agreement was judged to be satisfactory.

Roberg[10] simulated the flow of paper pulp in a cylindrical-stirred tank equipped with a side-entering mixer. The author assumed laminar flow throughout the vessel and used both Newtonian and non-Newtonian power law rheology models to describe the pulp suspension. Estimates for the axial and tangential forces produced by the impeller were distributed over the volume swept by the impeller blades and set as sources of momentum. The velocity fields obtained using the Newtonian and non-Newtonian rheological models were compared against each other and found to agree qualitatively, but not quantitatively. These profiles where not compared against experimental measurements.

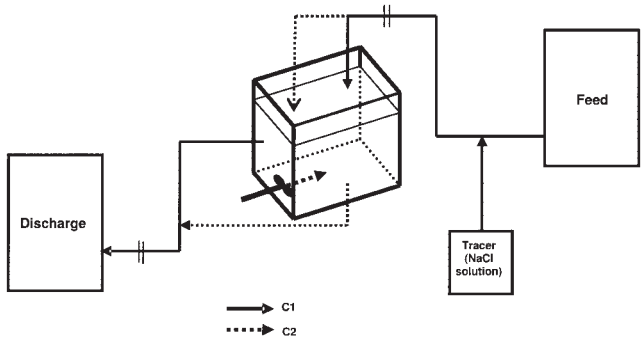

Figure 1. Experimental setup. Input-output configurations studied: C1 (solid lines) and C2 (dotted lines).

Wikstrom and Rasmuson[11] studied the agitation of pulp suspensions with a jet nozzle agitator using CFD. The impeller was modeled by imposing boundary conditions on the external flow, the pulp suspension was described as Bingham fluid, and flow inside the chest modeled as being laminar. Experimental velocity measurements in the tank were taken using sonar Doppler velocimetry at four positions inside the modeled chest. Wikstrom and Rasmuson found that the flow field obtained from the CFD calculations increasingly deviated from the velocities measured as the distance from the impeller increased. Since the CFD calculation underestimated the velocity far away from the agitator, they included a shear-thinning parameter by using a Herschel-Bulkley model for the suspension rheology. They found no significant improvement over the Bingham model, and suggested that pulp suspension behavior was not fully described by these models.

The objective of this work was to simulate pulp mixing in a scale-model stock chest utilizing commercial CFD software (Fluent 6.1) and a simple model for pulp suspension rheology. The velocity fields calculated from the steady-state simulations were used to determine the dynamic response of the model which was then compared with the experimental data obtained by Ein-Mozaffari et al.[12] In this way, the CFD model could be evaluated, and further avenues for improvement and refinement of the CFD simulations identified.

Experimental Techniques

The laboratory 1:11 scale-model chest used by Ein-Mozaffari et al. in their experimental studies was modeled here.[12] This chest (illustrated in Figure 1) was rectangular, with dimensions of width: $W = 40$ cm, length: $L = 53$ cm and height: $Z = 70$ cm. The dimensions of the computational domain are shown in Figure 2. The impeller studied was a scale version of the industrial Maxflo impeller (Chemineer, Inc., Dayton, Ohio) and had a diameter of 16.5 cm, and was offset from the wall by 7 cm. The tests compared in this article were made with a 3.3% FBK (fully bleached kraft) pulp suspension over a range of impeller speeds (N) from 1,000 to 1,600 rpm, and flow rates through the chest (Q) from 7.9 to 37.1 L/min. The effect of pulp inlet and exit locations was modeled for the two configurations shown in Figure 1. Detailed design information is available elsewhere.[13]

The commercial CFD software package, Fluent V6.1 (Flu-

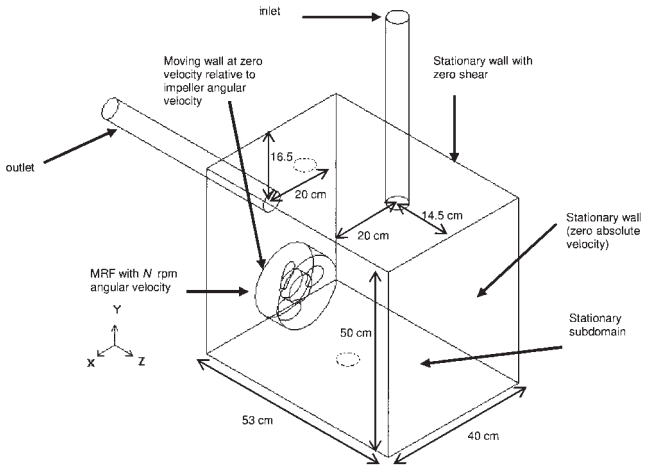

Figure 2. Dimensions and boundary conditions of the solution domain for Configuration 1.

The impeller is centered on the back wall 12 cm above the chest floor. The feed and exit locations for Configuration 2 are also shown in the figure as dashed openings. The feed is on the top surface, centered 12.5 cm in front of the impeller wall. The exit is on the bottom surface, centered 26.5 cm in front of the impeller wall.

ent, Inc., Lebanon, NH) was used to simulate the suspension flow within the mixing chest by solving the conservation of mass and momentum equations. The computational domain within the chest was discretized with multiblock mesh structures using Gambit software (v. 2.1.6, Fluent, Lebanon, NH). Gambit was also used to generate the three-dimensional (3-D) geometrical mesh for the impeller. In order to provide a more efficient allocation of the computational cells and to better capture the boundary layer effects, an increased mesh density was used near the vessel walls and the rotating impeller blades. The original 3-D mesh of the model had 1.1×10^5 computational cells, a combination of tetrahedral elements around the impeller blades, and hexahedral elements elsewhere. In order to ensure that the mesh was sufficiently refined in regions having large gradients of pressure and swirl velocity, a solution-adaptive refinement of the mesh was incorporated in our model. Assuming that the greatest error occurs in regions of high-velocity gradients in the vessel, features of the evolving flow field were used to drive the grid adaptation process in an automated dynamic refinement of the mesh on those cell zones with high-velocity gradients according to the procedure outlined in the Fluent users manual.[14]

The flow in the mixing chest is unsteady in an inertial frame of reference because the rotor/impeller blades sweep the domain periodically. However, in the absence of stators or baffles, it is possible to perform calculations in a domain that moves with the rotating impeller. In this case, the flow is steady relative to the rotating (noninertial) frame, and the velocity of the coordinate system is included in the equations of motion describing the flow.[15] In implementation of this numerical approach, known as the multiple reference frame (MRF), the calculation domain is divided into subdomains, each of which may be rotating with respect to the inertial frame. The governing equations in each subdomain are written with respect to the subdomain's reference frame, and the continuity of the absolute velocity is enforced at the boundaries between subdomains.

Figure 2 shows the solution domain for the mixing chest, and the locations of the boundary conditions for the mixing vessel. For the rotating and stationary subdomains, the angular velocity (Ω), and axis of rotation in each reference frame was specified. The rotation axis origin was located at the center of the impeller hub with its orientation in the positive z direction. The impeller speed was specified in the moving subdomain and the impeller blades were treated as walls that moved with zero-relative velocity. Likewise, the chest-walls were given a velocity of zero in the absolute reference frame. The velocity inlet was defined as having a flat profile 10 dia. upstream of the chest with a magnitude $|v| = 4Q/\pi D^2$, and a negative y orientation. The exit boundary condition was specified as fully developed flow at the end of a pipe with an L/D ratio of 10.

Pulp suspension rheology was approximated using the modified Herschel-Bulkley model available in Fluent. At very low-strain rates ($\dot{\gamma} \leq \tau_y/\mu_0$) the suspension is modeled as an extremely viscous fluid with viscosity μ_0. As a result, regions in the suspension that are stationary in reality have a very low-velocity in the CFD solution. This is done to avoid instability during computation. As the strain rate is increased and the yield stress τ_y, passed, suspension behavior is described using a power law. Therefore, the apparent viscosity of the suspension, μ, is given by

$$\mu = \mu_0 \qquad \text{for } \tau \leq \tau_y \tag{1a}$$

$$\mu = \frac{\tau_y + k\left[\dot{\gamma}^n - \left(\frac{\tau_y}{\mu_0}\right)^n\right]}{\dot{\gamma}} \qquad \text{for } \tau > \tau_y \tag{1b}$$

The consistency index k, was set to 0.001 Pa·s (the viscosity of water), and the power-law index n, to 1.0. The yield stress of the $C_m = 3.3\%$ FBK was set to $\tau_y = 475 \pm 62$ Pa,[16] and the viscosity up to the yielding point (the yielding viscosity) was estimated, based on experimental data collected by Bennington[7], as $\mu_o = 100 \pm 43$ Pa.s.

In general, the viscosity for non-Newtonian fluids is a function of all three invariants of the rate of deformation tensor $\bar{\bar{D}}$. However, for non-Newtonian liquids, μ can be considered to be a function of shear rate[17] $\dot{\gamma}$, which is related to the second invariant of $\bar{\bar{D}}$ and is defined as

$$\dot{\gamma} = \sqrt{\bar{\bar{D}}:\bar{\bar{D}}} \tag{2}$$

with $\bar{\bar{D}}$ given by

$$\bar{\bar{D}} = \left(\frac{\partial u_j}{\partial x_i} + \frac{\partial u_i}{\partial x_j}\right) \qquad i, j = 1, 2, 3 \tag{3}$$

Since suspension flow observed in the experiments is primarily laminar, the mass and momentum conservation equations were solved in the laminar regime using a second-order upwind scheme. (Although flow near the impeller might be turbulent, the fluctuation velocities will diminish quickly in the areas outside of the impeller zone due to the fibrous structure of the

suspension. Considering the flow as laminar in the entire domain will not impact the flow field significantly). Further, the non-Newtonian Reynolds number calculated for the impeller using the method of Gibbon and Attwood[18] and Blasinski and Rzyski[19] was below 10^3 and, therefore, in the laminar regime according to criteria used to characterize agitated vessels. To obtain converged solutions of the CFD model, calculations were started at low-impeller speeds, and the impeller speed gradually increased until the desired operating condition was reached. Iterations were continued until the scaled residuals for each transport equation were below 10^{-5}.

Spatial-grid independence was verified by demonstrating that additional grid lines near the impeller surface did not significantly change the calculated velocity magnitude measured in a line 8 cm in front of the impeller centered on the impeller hub. This location was chosen because it is critical for the numerical solution as the highest velocity gradients and mass imbalance residuals were located in this area. The final dynamic adapted mesh used (which contained 202,010 cells) was further refined performing one and two additional velocity gradient adaptations (426,520 and 786,422 cells, respectively). Increasing the number of cells by a factor of four did not change the velocity magnitude in front of the impeller by more than 3%. Computations were carried out using a 2.4 GHz Pentium 4 CPU with 1.0 GB of RAM. Second-order convergence was typically achieved after 3–5 h.

There are a number of model-based errors possible in this work, including physical approximation errors (for example, physical modeling errors, geometry modeling errors), and numerical approximation errors (for example, spatial and temporal discretization errors, iterative convergence errors, computer round-off errors). In our study, since mesh independent results were achieved and the convergence criteria were relatively small, numerical approximation error is not expected to be significant. The modeling errors can be evaluated by comparing the simulation results with measured dynamic data. This was accomplished by creating time-dependent solutions to the steady-state model results and comparing the model output directly with the experimental measurements, or by fitting both the simulation and experimental data sets to an independent black-box mixing model and comparing model parameters.

The black-box dynamic model was developed[12] based on the observed nonideal behavior of industrial pulp chests

$$G_{chest} = \frac{fe^{-T_{is}}}{1+\tau_1 s} + \frac{(1-f)(1-R)\dfrac{e^{-T_{2s}}}{1+\tau_2 s}}{1-\dfrac{Re^{T_{2s}}}{1+\tau_2 s}} \qquad (4)$$

where G_{chest} is the transfer function of the chest. The model includes a well mixed zone (represented by a first-order transfer function having a time constant τ_2 and time delay T_2), as well as the possibility of stock recirculation R, within that mixing zone. A fraction of the entering flow f, could by-pass the primary mixing zone and pass directly to the exit, although it could be involved in some limited mixing. Thus, a first-order transfer function with time constant and delay (τ_1 and T_1) was included for this portion of the flow. To estimate the model parameters the system was excited. The choice of excitation signal has a substantial influence on the accuracy with which the parameters could be estimated. A frequency modulated random binary signal was designed to provide excitation of the system at the critical chest frequencies.[12]

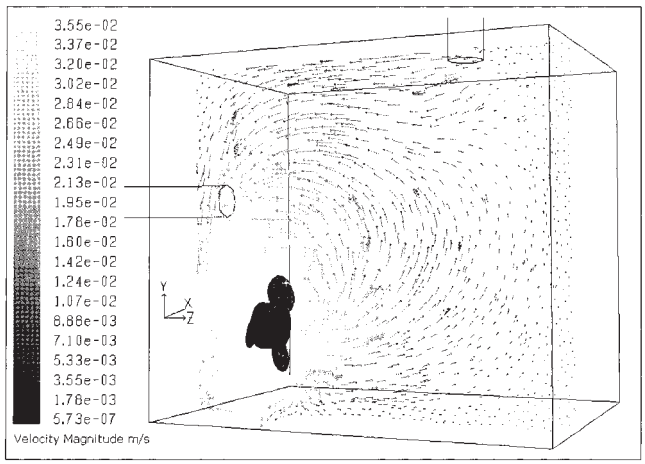

Figure 3. Velocity vectors (arrows) calculated on the plane $x = 0$ cm (impeller plane) using CFD. $C_m = 3.3\%$ FBK suspension at $Q = 37.1$ L/min and $N = 1203$ rpm.

Vector lengths are scaled according to the magnitude of the calculated velocity. Details in the impeller zone have been omitted for clarity.

The pseudo random binary input used by Ein-Mozaffari et al. for the experimental tests was simulated in Fluent using a user-defined function written in the C programming language. To obtain raw data that could be directly compared with the experimental measurements, the mass fraction input concentration of tracer was set to a value analogous to the measured conductivity values (as conductivity is proportional to mass concentration) and the input/output data recorded. The discretization step size Δt was initially set one-order of magnitude smaller than the time constant estimated for the mixing system, and was then further reduced to ensure convergence after 20–30 iterations at each time step.[14] Dynamic data obtained using different step sizes at each flow rate were compared to verify discretization independency. For example, at $Q = 37.1$ L/min, the model-generated dynamic response was compared with sampling intervals of $\Delta t = 1$ and 0.5 s. The predicted responses overlapped, indicating temporal independence. Similar results were found for tests made at $Q = 7.9$ L/min for time-step sizes of 5 and 2.5 s. It turns out that the sampling intervals chosen for obtaining the dynamic response of the virtual system were identical to those used by Ein-Mozaffari et al.[12] for acquiring the original experimental data. The dynamic parameters were estimated from the input-output data using the numerical method described by Kammer et al.[20]

Results and Discussion

The CFD simulation results for an inlet flow rate of $Q = 37.1$ L/min and an impeller angular velocity of $N = 1203$ rpm, are shown in Figure 3. The qualitative agreement between the calculated and the observed flow fields (taken under identical operating conditions) on the visible surfaces of the mixing chest was good as shown in Figures 4 and 5. Arrows are used

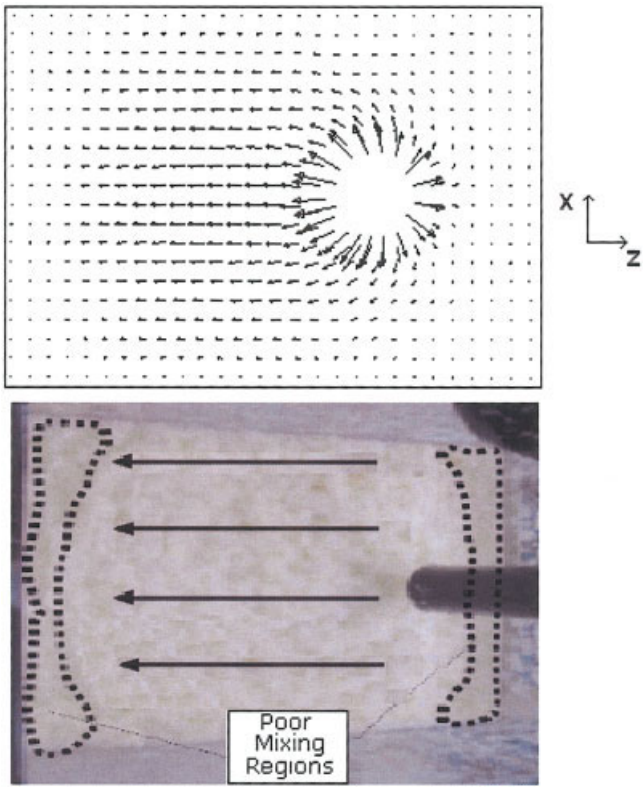

Figure 4. Velocity vectors calculated on the top surface of the mixing chest using CFD (top image).

C_m = 3.3% FBK suspension at Q = 37.1 L/min and N = 1203 rpm. The bottom figure shows a photograph with the observed suspension motion given by arrows. The dotted lines indicate regions of very slow suspension movement. [Color figure can be viewed in the online issue, which is available at www.interscience.wiley.com.]

to indicate the observed direction of suspension motion in these still photos. Under the test conditions the entire suspension was in motion. However, poor mixing regions still existed at the bottom of the chest along the wall opposite to the impeller, and at the top surface of the suspension along the walls adjacent to and opposite of the impeller. In these locations pulp flow was significantly slower than in the bulk zone. Pulp remained for a long time in these regions which effectively decreased the percentage of fully mixed volume within the chest.

The power input to the impeller (P) was calculated from the CFD simulation data using $P = 2\pi NM$ where M is the moment vector about the center of the impeller. The calculated power input matched the experimentally determined values well, as shown in Figure 6, particularly at high-impeller speeds where the deviation was as low as 1%. For all the conditions studied, the values were over-predicted by CFD although the dependence of power input as a function of rotation speed was very similar. This discrepancy may be due to a number of the assumptions made in the simulation, including: the rheological model chosen to describe suspension rheology, the use of the laminar-flow model in the region near the impeller, and/or the inability of the model to capture the small recirculation zones and swirls near the blade tips. However, the improved agreement between the computed and measured power input at the highest impeller speed suggests that at higher-shear rates the non-Newtonian viscosity calculated by the modified Bingham model approached that of the actual suspension more closely.

The dynamic tests conducted by Ein-Mozaffari et al.[4] were simulated numerically using virtual tracer addition, and the transient solution of the species conservation equation. After obtaining the velocity field by solving the transport equations, tracer particles having identical properties to that of the pulp suspension were uniformly distributed at the inlet and tracked through the flow domain. The particle trajectories, representing the flow path lines, are computed based on the steady continuous-phase flow field. Figure 7 shows the paths followed by tracer particles in one simulation. As clearly shown by the

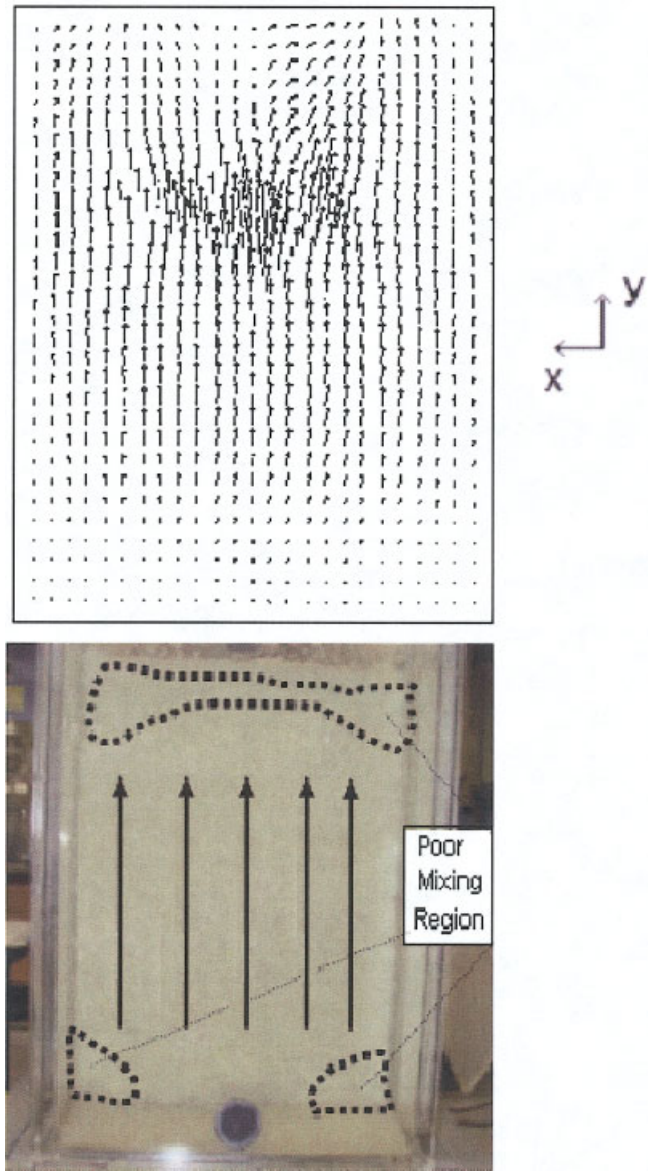

Figure 5. Velocity vectors on the wall opposite the impeller.

C_m = 3.3% FBK suspension at Q = 37.1 L/min and N = 1203 rpm. The bottom figure shows a photograph with the observed suspension motion given by arrows. The dotted lines indicate regions of very slow suspension movement. [Color figure can be viewed in the online issue, which is available at www.interscience.wiley.com.]

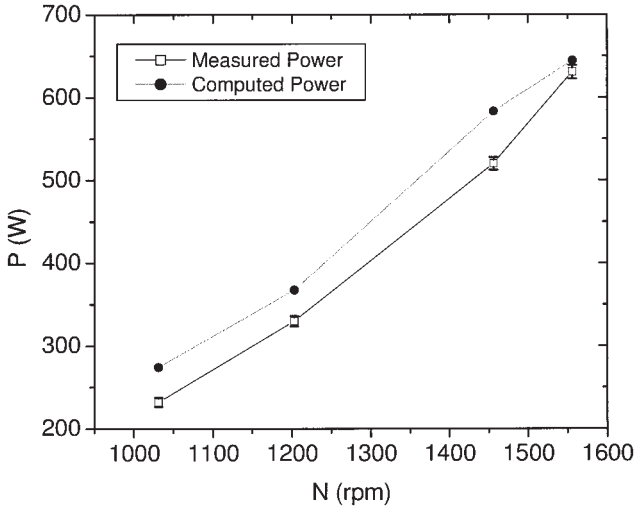

Figure 6. Calculated and measured power input vs. impeller rotational speed.

C_m = 3.3% FBK suspension at Q = 37.1 L/min. The representative error bars are based on the accuracy of the torque meter (± 0.05 Nm) used to measure the experimental data.

particle trajectories, a significant number bypass the mixing zone and end up at the outlet, resulting in undesirable channeling through the mixing chest.

A comparison between the experimentally measured dynamic tests (gray lines) and the computed responses for identical conditions (black lines) for a C_m = 3.3% FBK suspension for a number of conditions are given in Figure 8. In each figure, the upper pair of lines corresponds to the input signal and the lower pair of lines corresponds to the output response. The excitation signal used in the simulations did not include noise present in the experimental signals and, thus, the numerical output is smooth. The computed responses agree with the measured data very well, although some details differ as discussed later.

Figure 8a compares experimental and computational results

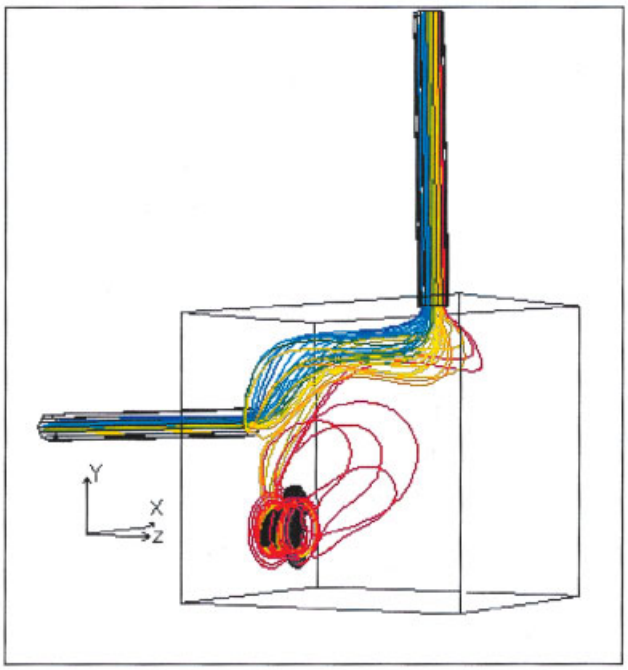

Figure 7. Trajectories of tracer particles released at the inlet. Conditions as given in Figure 4.

[Color figure can be viewed in the online issue, which is available at www.interscience.wiley.com.]

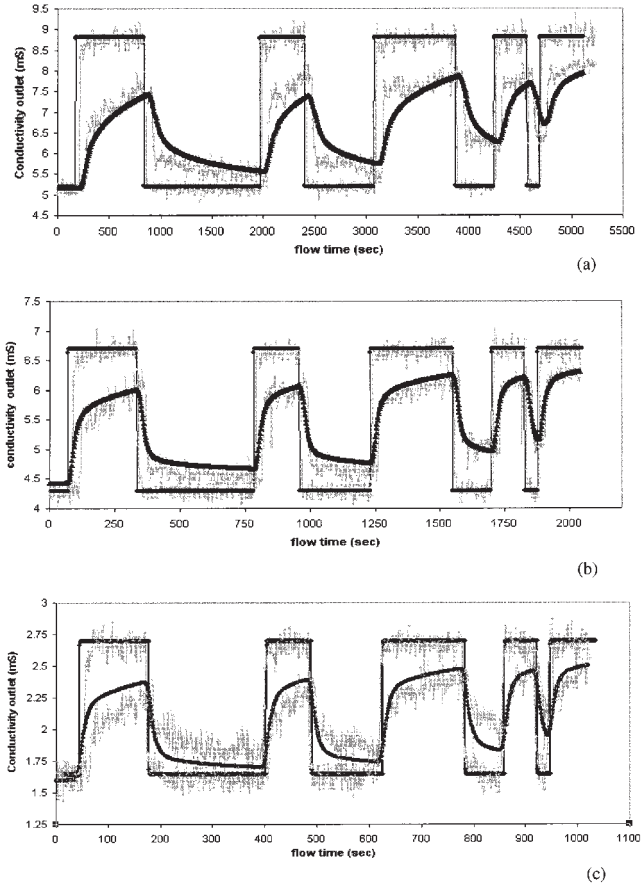

Figure 8 Input (upper)/output (lower) signals for numerical (black) and experimental (gray) measurements for the scale-model chest in configuration C1.

C_m = 3.3% FBK: (a) Q = 7.9 L/min, N = 1031 rpm; (b) Q = 21.1 L/min, N = 1031 rpm; (c) Q = 37.1 L/min, N = 1456 rpm. Note that the absolute magnitude of the signal (y-axis) changes depending on the total concentration of tracer in the suspension at the time of the test.

Table 1. Comparison of the Parameters Estimated from Experimental and CFD Data

Dynamic Parameters	Experiment Q = 7.9 L/min, N = 1031 rpm	CFD Q = 7.9 L/min, N = 1031 rpm	Experiment Q = 21.1 L/min, N = 1031 rpm	CFD Q = 21.1 L/min, N = 1031 rpm
f	0.51	0.44	0.57	0.59
T_1 (s)	55	35	22	20
τ_1 (s)	11.4	65	5.4	22.5
T_2 (s)	170	230	74	96
τ_2 (s)	1150	1245	400	493

C_m = 3.3% FBK at Q = 7.9 L/min and Q = 21.1 L/min for N = 1031 rpm. Configuration C1.

Table 2. Comparison of the Parameters Estimated from Experimental and CFD Data

Dynamic Parameters	Experiment	CFD	Experiment	CFD
Q = 37.1 L/min	N = 1203 rpm		N = 1456 rpm	
f	0.83	0.66	0.35	0.60
T_1 (s)	14	13	10	12
τ_1 (s)	1.8	14.9	3.0	14.5
T_2 (s)	108	91	25	26
τ_2 (s)	133	324.4	167.0	366.5
Q = 7.9 L/min	N = 1258 rpm		N = 1456 rpm	
f	0.35	0.50	0.14	0.36
T_1 (s)	45	60	45	30
τ_1 (s)	13.3	75.5	14	32
T_2 (s)	140	295	90	50
τ_2 (s)	966.1	1413.1	814	1221

C_m = 3.3% FBK at Q = 37.1 L/min and Q = 7.9 L/min for different impeller speeds. Configuration C1.

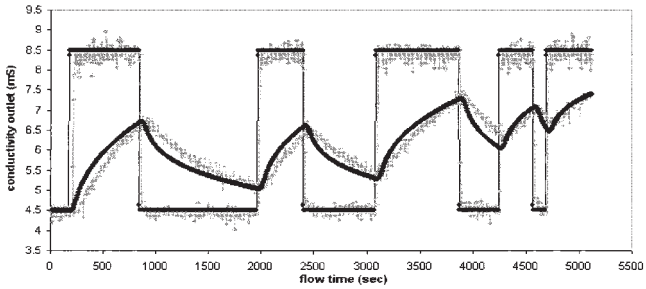

Figure 9: Input (upper)/output (lower) signals for numerical (black) and experimental (gray) measurements for the scale-model chest in configuration C2.

C_m = 3.3% FBK at Q = 7.9 L/min and N =1105 rpm.

for a flow rate of Q = 7.9 L/min through the mixing chest. The calculated dynamic response agrees fairly well with the measured response, particularly for the first-step change. The computed response shows an exponential conductivity rise, while the experimentally-measured response shows a more abrupt step change. This is attributed to the high-degree of channeling in the system, with the simulation predicting a greater extent of mixing in the bypassing flow present.

As the flow rate through the chest is increased to Q = 21.1 and Q = 37.1 L/min (Figure 8 b and c), the CFD predictions show better agreement with the experimental data. However, a trend is observed whereby the dynamic response calculated is below the measured output at the lowest-flow rate (Figure 8a), closely predicted at the modest flow rate (Figure 8b), and over predicted at the highest-flow rate (Figure 8c). Despite these deviations, the simulated predictions approximate the experimental response to a good extent. Thus, the mixing dynamics in the scale model chest are reasonably predicted from the velocity field calculated in the CFD simulations. This constitutes a valuable technique for evaluation of the CFD model developed.

The dynamic behavior predicted using the CFD simulations was also compared using the parameters for the black box dynamic model. The data in Table 1 tabulates parameters for the tests given in Figures 8a and b. It can be seen that at higher-feed rates (Q) the system is prone to a higher degree of channeling (f increased as Q was increased when all other factors were kept constant). All the parameters calculated from the CFD are in the same range as the experimentally measured ones, except for the time constant of the bypassing flow, τ_1. Even though τ_1 is much smaller than τ_2, the value calculated from the CFD data is about five times larger than that obtained from the experimental data, suggesting that a considerably higher-degree of mixing is calculated for the bypass flow than found experimentally.

The effect of the impeller speed on system dynamics was also examined. Table 2 compares the parameters calculated for the simulation with those measured experimentally for C_m = 3.3% FBK at different impeller speeds, and two suspension flow rates (Q = 37.1 and 7.9 L/min). The data show that channeling decreases as impeller speed increases. At higher-impeller speeds the suspension network is disrupted further away from the impeller, which leads to improved mixing by reducing the extent of nonideal flow in the system.[21]

The dynamic tests performed by Ein-Mozaffari et al.[12] show that pulp feed and exit locations significantly affect the degree of upset attenuation obtained in the mixing chest. For example, the dynamic performance of the scale chest was improved by changing the feed and exit locations to that of configuration C2 as illustrated in Figure 1. The flow patterns for C1 (see Figures 3, 4 and 5) show that a large percentage of the pulp feed can easily channel when it moves on the surface of the chest toward the exit location on the impeller wall without being forced into the mixing zone by the impeller. On the other hand, configuration C2 forces the surface flow through the mixing zone before leaving the chest.

Model and experimental input/output data for configuration C2 at Q = 7.9 L/min and N = 1105 rpm are compared in Figure 9. The measured and simulated output data agree fairly well. Both signals show a progressive change in exiting suspension conductivity that follows the changes given by the excitation signal, with the simulated response having greater exponential character than the experimental data. This seems to follow the pattern observed with the previous configuration. For configuration C2, the dynamic response is modeled by T_2 and τ_2 alone, as shown in Table 3. The time constant of the mixing zone is under predicted by 8% at the lower impeller

Table 3. Comparison of the Parameters Estimated from Experimental and CFD Data

Dynamic Parameters	Experiment	CFD	Experiment	CFD	Experiment	CFD
	N = 1031 rpm		N = 1105 rpm		N = 1557 rpm	
f	0	0	0	0	0	0
T_2 (s)	40	10	45	10	40	12
τ_2 (s)	684	623	708	673	789	694

C_m = 3.3% FBK at Q = 7.9 L/min and different impeller speeds for configuration C2.

speed and under predicted by 11% at the higher-impeller speed. Under identical operating conditions, the time constant and time delay of the mixing zone for both numerical and experimental data are much lower for C2 than for C1. Thus, the system given by C2, despite having considerably less delay, responds more slowly to changes in the input signal but provides greater attenuation of high-frequency variability.

Conclusions

A CFD model of a rectangular pulp-stock mixing chest was developed using Fluent v6.1 with the rheology of the pulp suspension approximated using a modified Bingham plastic model. A procedure was developed to determine the dynamic response of the numerical simulation and compare it with experimental data. Using this technique, it was shown that the numerical model captured the mixing dynamics of the scale-model chest fairly well, although it overestimated the exponential extent of mixing in the chest. This is particularly noticeable in flow situations containing significant bypassing, where the model overestimates the extent of mixing in the bypassing flow. Departure of the simulated and measured dynamics is attributed to the rheology of the suspension, which is not fully described by the model used.

Notation

D = impeller diameter, m
$\bar{\bar{D}}$ = rate of deformation tensor
f = percentage of channeling, fraction
G_{chest} = transfer function for the pulp stock chest
k = consistency factor, Pa.s
M = torque, N.m
n = power-law index
N = impeller rotational speed, s^{-1}
P = power, W
Q = pulp flow rate through the chest, m^3/s
R = percentage of recirculation, fraction
T_1 = time delay for the channeling zone, s
T_2 = time delay for the agitated zone, s

Greek letters

$\dot{\gamma}$ = shear rate, s^{-1}
μ = viscosity, Pa.s
μ_0 = yielding viscosity, Pa.s
ρ = fluid density, kg/m^3
τ = shear stress, N/m^2
τ_1 = time constant for the channeling zone, s
τ_2 = time constant for the mixing zone, s
τ_y = yield stress, N/m^2
Ω = angular velocity, rpm

Literature Cited

1. Bialkowski WL. Newsprint variability and its impact on competitive position. *Pulp Pap Can*. 1992;93(11):T299−T306.
2. Yackel, DC. *Pulp and paper agitation: the history, mechanics and process*. Atlanta: TAPPI Press; 1990.
3. Oldshue JY, Gretton AT. Performance and design of paper stock mixers. *Tappi J*. 1956;39(6):378−390.
4. Ein-Mozaffari F, Bennington CPJ, Dumont GA. Performance and design of agitated pulp stock chests. *Appita J*. 2003;56(2):127−133.
5. Ein-Mozaffari F, Bennington CPJ, Dumont GA. Dynamic mixing in agitated industrial pulp chests. *Pulp Paper Can*. 2004;105(5): T118−T122.
6. Wikstrom T. *Flow and rheology of pulp suspensions at medium consistency*. Chalmers University of Technology; 2002. PhD Thesis.
7. Bennington CPJ. *Mixing pulp suspensions.* University of British Columbia, 1988. PhD Thesis.
8. Brucato A, Ciofalo M, Grisfi F, Micale G. Numerical prediction of flow fields in baffled stirred vessels: a comparison of alternative modeling approaches. *Chem Eng Sci.* 1998;53:3653−3684.
9. Bakker A, Fasano JB. A computational study of the flow pattern in an industrial paper pulp stock chest with a side-entering impeller. *AIChE Symposium Series*. 1997;89(293):118−124.
10. Roberg KE. Numerical simulations of the flow of fibre suspension in a side-entering mixer. *Récents Progrès en Génie des Procédés.* 1997; 11(51):203-210.
11. Wikstrom T, Rasmuson A. The agitation of pulp suspension with a jet nozzle agitator. *Nordic Pulp Pap Res J*. 1998;13(2):88−94.
12. Ein-Mozaffari F., Kammer LC, Dumont GA, Bennington CPJ. Dynamic modeling of agitated pulp stock chests. *Tappi J*. 2003;2(9):13-17.
13. Ein-Mozaffari F. *Macroscale mixing and dynamic behaviour of agitated pulp stock chests.* University of British Columbia, 2002. PhD Thesis.
14. Fluent 6.1 User's Guide Documentation. Fluent Inc., Lebanon, NH; 2003.
15. Luo JY, Gosman AD, Issa RI. Prediction of impeller induced flows in mixing vessels using multiple frames of reference. *Inst Chem Eng Symp Ser*. 1994;136:549−556.
16. Ein-Mozaffari F, Bennington CPJ, Dumont GA. Suspension yield stress and the dynamic response of agitated pulp chests. *Chem Eng Sci*. 2005;60:2399-2408.
17. Bird RB, Armstrong RC, Hassager O. *Dynamics of Polymeric Liquids*. Volume 1: *Fluid. Mechanics*. Vol. 1. 2nd ed.Wiley Interscience, New York; 1987.
18. Gibbon JD, Attwood D. Prediction of power requirements in the agitation of fiber suspsnsions. *Trans Inst Chem Engrs*. 1962;40:75-82.
19. Blasinski H, Rzyski E. Mixing of non-Newtonian liquids. Power consumption for fibrous suspensions. *Inz Chem*. 1972;2(1):169-182.
20. Kammer LC, Ein-Mozaffari F, Dumont GA, Bennington CPJ. Identification of channeling and recirculation parameters of agitated pulp stock chests. *J Process Control.* 2005;15(1):31-38.
21. Bennington CPJ. Kerekes RJ, Grace JR. The yield stress of fibre suspensions. *Can J Chem Eng*. 1990;68:748−757.

Manuscript received May 4, 2005, and revision received Jun. 6, 2006.